Thin-Walled Structures 189 (2023) 110903

Contents lists available at ScienceDirect

Thin-Walled Structures

journal homepage: www.elsevier.com/locate/tws

Full length article

Optimization of graphene/fibre reinforced cantilever skew laminates for maximum fundamental frequency via non-uniform distribution of reinforcements

Y. Jeawon [a], G.A. Drosopoulos [b,a,*], G. Foutsitzi [c], G.E. Stavroulakis [d], S. Adali [e]

[a] Discipline of Civil Engineering, University of KwaZulu-Natal, Durban, South Africa
[b] Discipline of Civil Engineering, University of Central Lancashire, Preston, UK
[c] Department of Informatics and Telecommunications, University of Ioannina, Ioannina, Greece
[d] School of Production Engineering and Management, Technical University of Crete, Chania, Greece
[e] Discipline of Mechanical Engineering, University of KwaZulu-Natal, Durban, South Africa

ARTICLE INFO

Keywords:
Optimal design
Graphene reinforcement
Vibration
Finite element analysis
Skew cantilever laminates

ABSTRACT

Three-phase graphene/fibre-reinforced cantilever skew laminates are optimized with the design objective of maximizing the fundamental frequency. Four optimal design problems are formulated involving one, two, three, and four design variables: graphene content, fibre content, layer thicknesses, and the fibre orientations. Optimization is implemented using a Sequential Quadratic Programming optimization algorithm within finite element analysis. It is observed that optimizing the graphene and fibre contents across the thickness leads to increased fundamental frequency. A trend is observed for the frequency of skew laminates to increase but for their design efficiency to decrease compared to rectangular laminates.

1. Introduction

The use of laminated rectangular and skew plates as structural components has increased due to their significant advantages. These include high strength/weight and high stiffness/weight ratios compared to conventional materials. Composite plates, used as lightweight components, are often exposed to severe vibrations. In this case, a critical issue is to avoid resonance when the natural frequency of the laminate coincides with the excitation frequency. Avoiding resonance becomes particularly important in aerospace applications due to weight limitations. One of the methods adopted to resolve this issue is to design a laminate such that its fundamental frequency is higher than the excitation frequency. This approach leads to an optimal design problem with the objective of maximizing the fundamental frequency for a given weight of the laminate.

One of the recently introduced technologies to produce lightweight composites is to use nanoscale reinforcements which have high stiffness–weight ratios compared to traditional fibre reinforcements. Currently, carbon nanotubes (CNTs) and graphene nanoplatelets (GPLs) are among the most widely used nanomaterials introduced as reinforcements. Due to their excellent mechanical properties, a small amount of nano reinforcement can substantially improve the mechanical properties and the vibration response of the laminates.

Several studies on skew plates' vibration response have been reported in the literature. Vibrations of skew laminates with cut-outs were studied in [1], and the vibrations of laminated skew plates with and without cut-outs in [2]. Vibrations of skew cantilever plates with stiffeners were studied in [3] to observe the differences in the frequencies compared to rectangular plates. Results indicated that cantilever skew plates provide improved flexural rigidity as compared to rectangular plates. Vibrations of laminated cantilever trapezoidal plates were the subject of the study in [4]. In [5,6], free vibrations of skew laminates were studied, and it was observed that as the skew angle increases, the natural frequency also increases. In [7], an investigation of the free vibrations of skew plates indicated an increase of the fundamental frequency with increasing skew angle, aspect ratio and width to thickness ratio. In [8], vibrations of laminated skew plates were studied, and it was observed that the frequency increases with increasing skew angle.

Several studies focused on the response of graphene or carbon nanotube-reinforced laminates known as two-phase nanocomposites. Vibrations of functionally graded and carbon nanotube reinforced skew laminates were studied in [9–12]. The effects of nanotube content on the frequencies of skew laminates were investigated in [13], and the impact of carbon nanotube waviness and agglomeration on the vibrations of skew laminates in [14]. The vibration response of skew plates with varying stiffness was studied in [15], and it was observed that an increase in the skew angle increased the fundamental frequency confirming the previous results.

* Corresponding author at: Discipline of Civil Engineering, University of Central Lancashire, Preston, UK.
E-mail address: gdrosopoulos@uclan.ac.uk (G.A. Drosopoulos).

https://doi.org/10.1016/j.tws.2023.110903
Received 24 February 2023; Received in revised form 18 May 2023; Accepted 23 May 2023
Available online xxxx

Several studies involved the vibrations of functionally graded graphene nanoplatelet-reinforced two-phase composites. The studies [16–19] observed that a small increase in the graphene content increased the fundamental frequency substantially. Functionally graded graphene-reinforced plates subject to thermal and mechanical loads were investigated in [20]. This study also indicated that adding a small amount of graphene leads to a considerably higher fundamental frequency.

Several investigations studied the optimal design of skew laminates. Optimization of skew laminates to maximize the frequency was the subject of the paper [21], with the study based on the first-order shear deformation theory. It was observed that as the skew angle increased, the optimal fibre orientations increased and for large enough skew angles, the influence of the fibre orientations became insignificant. Fundamental frequencies of symmetric and anti-symmetric skew laminates were maximized in [22] by determining the optimal stacking sequence. Genetic algorithms, particle swarm optimization and cuckoo search methods were used in [23] to maximize the fundamental frequency of skew plates.

The vibrations of graphene-reinforced skew plates on point supports were studied in [24]. The nonlinear vibration response of graphene-reinforced beams was studied in [25] and it was observed that the non-uniform distribution of graphene across thickness yielded better results as compared to the uniform distribution of graphene. The effect of graphene nanoplatelets on a polymer composite was studied in [26] and it was noted that a proper alignment of the nanoplatelets significantly improved the mechanical response compared to randomly orientated GPLs.

Recently, the mechanical response of three-phase composites using GPLs or CNTs and with glass or carbon fibre reinforcements in a polymer matrix has been investigated. These studies aim to balance the benefits of nanoscale reinforcements to achieve lower weight and higher stiffness with the increased cost of using nano materials. An investigation on the optimization of three-phase graphene/fibre-reinforced rectangular laminates with the objective of maximizing the fundamental frequency was presented in [27]. Design variables used in this study were the graphene content, the fibre content, the layer thicknesses and the fibre orientations and the numerical results were given only for the simply supported and clamped boundary conditions. Results highlighted the improvement of the design efficiency by introducing optimal non-uniform distributions of graphene and fibre reinforcements across the laminate thickness. The vibration response of three-phase, graphene/carbon fibre-reinforced laminates was studied in [28], emphasizing the contribution of graphene reinforcement to increase the fundamental frequency. In [29], the influence of using graphene reinforcement in addition to carbon or glass fibres on the buckling response of angle-ply laminates was evaluated. Results indicated that an increase in the graphene content led to substantially higher buckling loads.

Based on the literature study and according to authors' best knowledge, no research has been conducted on optimizing the fundamental frequency of three-phase graphene/fibre-reinforced skew cantilever laminates. The present article involves the optimal designs of three-phase, skew cantilever laminates using four design parameters. Both graphene nanoplatelets and glass or carbon fibres are used as reinforcements leading to three-phase laminates. Design variables include the graphene and fibre contents of layers, the thickness of each layer and the fibre orientations. The overall scheme is implemented in MATLAB using finite element analysis. A design efficiency factor is introduced to provide a quantitative criterion to compare and assess the results of different optimal designs and the effectiveness of the design parameters. The vibration response and the design efficiency of three-phase skew and rectangular plates are also evaluated for comparison purposes.

Sections 2 and 3 of the article provide basic constitutive equations and the finite element formulation adopted in this work. The effective material properties using micromechanics equations are given in Section 4. Section 5 presents the optimal design problems, formulated for an increasing number of design variables. The verification of the proposed scheme by comparison with published literature and commercial finite element software is provided in Section 6. Sections 7 and 8 present the investigation's results, discussions, and conclusions.

2. Basic equations

The geometry of the skew plate under consideration is shown in Fig. 1. The length, width and thickness of the plate are defined as a, b and D in the x, y and z directions, respectively. Clamped boundary conditions are imposed on one side of the skew plate with a length equal to b (Fig. 1). The remaining three edges have free boundary conditions. The laminate consists of N layers with θ_k denoting the angle between the principal material direction and the coordinate x of the kth lamina. The mid-plane of the laminate coincides with the xy plane as shown in Fig. 1. The skew angle of the laminate is denoted by α. The coordinates of the bottom and top of the kth layer are denoted as $z = z_k$ and $z = z_{k+1}$ in the thickness direction.

2.1. Kinematics

The kinematics of the composite plate are formulated using the first-order shear deformation theory (FSDT) with the displacement field defined as:

$$u_1(x,y,z,t) = u(x,y,t) - z\varphi_x(x,y,t) \tag{1a}$$

$$u_2(x,y,z,t) = v(x,y,t) - z\varphi_y(x,y,t) \tag{1b}$$

$$u_3(x,y,z,t) = w(x,y,t) \tag{1c}$$

where $\{u\} = \{u_1, u_2, u_3\}^T$ is the displacement vector and $\{\bar{u}\} = \{u, v, w, \varphi_x, \varphi_y\}^T$ indicates the vector of generalized displacements in terms of the three mid-plane displacements and the normal rotations about the x and y-axes. The strain vector is given by:

$$\{\varepsilon\} = \nabla_S \{\bar{u}\} \tag{2}$$

where $\{\varepsilon\} = \{\varepsilon_{xx}, \varepsilon_{yy}, \gamma_{xy}, \gamma_{yz}, \gamma_{xz}\}^T$ and ∇_S is defined as

$$\nabla_S = \begin{bmatrix} \partial/\partial x & 0 & 0 & -z\partial/\partial x & 0 \\ 0 & \partial/\partial y & 0 & 0 & -z\partial/\partial y \\ \partial/\partial y & \partial/\partial x & 0 & -z\partial/\partial y & -z\partial/\partial x \\ 0 & 0 & \partial/\partial y & 0 & -1 \\ 0 & 0 & \partial/\partial x & -1 & 0 \end{bmatrix} \tag{3}$$

2.2. Constitutive equations

The constitutive equation of the kth lamina is expressed as:

$$\{\sigma\}_k = [Q]_k \{\varepsilon\} \tag{4}$$

where $\{\sigma\}$ is the stress vector and $[Q]$ is the elastic stiffness matrix. Under plane-stress conditions, the non-zero components $Q_{ij}^{(k)}$ of the elastic stiffness matrix for an orthotropic material are given by [30]:

$$Q_{11}^{(k)} = \frac{E_1^{(k)}}{\left(1 - v_{12}^{(k)} v_{21}^{(k)}\right)}, \quad Q_{12}^{(k)} = \frac{v_{12}^{(k)} E_2^{(k)}}{\left(1 - v_{12}^{(k)} v_{21}^{(k)}\right)} = Q_{21}^{(k)},$$

$$Q_{22}^{(k)} = \frac{E_2^{(k)}}{(1 - v_{12}^{(k)} v_{21}^{(k)})},$$

$$Q_{66}^{(k)} = G_{12}^{(k)}, \quad Q_{44}^{(k)} = k_s G_{23}^{(k)}, \quad Q_{55}^{(k)} = k_s G_{13}^{(k)} \tag{5}$$

In the above equations, $E_1^{(k)}$, $E_2^{(k)}$ are the longitudinal and transverse moduli, $v_{12}^{(k)}, v_{21}^{(k)}$ denote the Poisson's ratios, $G_{12}^{(k)}, G_{23}^{(k)}, G_{13}^{(k)}$ denote the shear moduli of the kth layer and k_s is the shear correction factor taken as 5/6. The elastic coefficient $Q_{ij}^{(k)}$ in the material coordinates

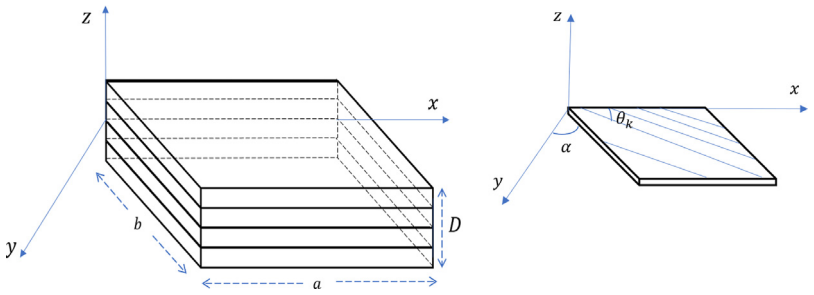

Fig. 1. Geometry of the laminated skew plate.

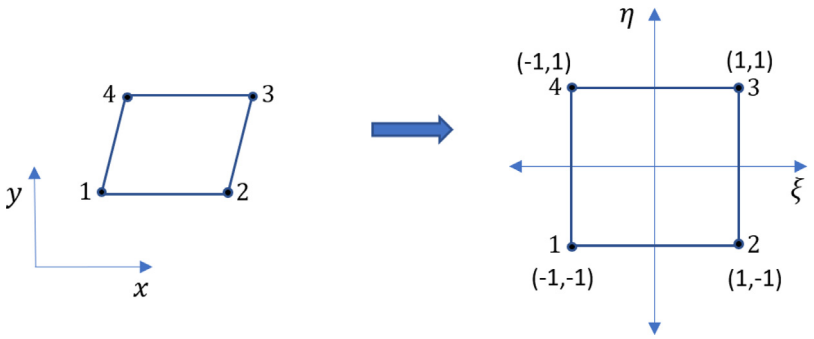

Fig. 2. Transformation of an isoparametric element from Cartesian (global) coordinates to natural (local) coordinates.

can be transformed into the coefficients $\overline{Q}_{ij}^{(k)}$ referred to the laminate coordinate system (x, y, z) using the relation:

$$\left[\overline{Q}\right]_{(k)} = \left([L]^T [Q] [L]\right)_{(k)} \tag{6}$$

where $[L(\theta_k)]$ is a transformation matrix and θ_k is the fibre orientation of the kth lamina as shown in Fig. 1 [30].

3. Finite element formulation

To solve the vibration problem, the finite element method is used. For skew plates, the borders of the elements are not parallel to the global axes of the plate as shown in Fig. 2. In the present study, isoparametric elements are utilized due to their capacity to simulate an arbitrary geometry accurately. The skew plate is discretized using four-noded isoparametric quadrilateral elements with five degrees of freedom (DOF) per node. Using these elements, the global coordinates x and y are related to the natural coordinates ξ and η as follows:

$$x(\xi,\eta) = \sum_{j=1}^{4} N_j(\xi,\eta)\, x_j, \quad y(\xi,\eta) = \sum_{j=1}^{4} N_j(\xi,\eta)\, y_j \tag{7}$$

where the Lagrange interpolation functions N_j are given by

$$N_j(\xi,\eta) = \frac{1}{4}\left(1+\xi_j\xi\right)\left(1+\eta_j\eta\right) \tag{8}$$

In Eq. (8), x_j, y_j are the coordinates of the node j in the cartesian (physical) domain and ξ_j, η_j are the coordinates of the node j in the natural (computational) domain as shown in Fig. 2. The same interpolation functions are used to define the generalized displacement vector within an element as

$$\begin{aligned}\left\{\overline{u}(x,y,t)\right\} \equiv \left\{u, v, w, \varphi_x, \varphi_y\right\}^T &= \sum_{j=1}^{4}\left(N_j(\xi,\eta)\,[I]_{5\times5}\left\{d_j(t)\right\}_e\right)\\ &= \left[N_u\right]\{d(t)\}_e\end{aligned} \tag{9}$$

where $\left\{d_j\right\}_e = \left\{u_j, v_j, w_j, \varphi_{xj}, \varphi_{yj}\right\}^T$ is the nodal displacement vector at the jth node of the element e and $[I]_{5\times5}$ denotes the 5×5 identity matrix.

Substituting Eq. (9) into (2) gives:

$$\{\varepsilon(x,y,t)\} = \nabla_S\left([H]\left[N_u\right]\{d\}_e\right) = [B]\{d\}_e \tag{10}$$

where $[B]$ is the strain–nodal displacement matrix.

3.1. Governing equations

The equations governing the dynamic response and the variationally consistent boundary conditions of the composite plate shown in Fig. 1, are derived using Hamilton's principle

$$\int_{t_1}^{t_2} (\delta T - \delta U + \delta W)\, dt = 0 \tag{11}$$

where T is the kinetic energy, U is the strain energy and W is the work done by external forces. At the initial and final times t_1 and t_2, the first variations vanish. The energy terms in Eq. (11) are defined as follows:

$$\begin{aligned} T &= \frac{1}{2}\int_V \rho\{\dot{u}\}^T\{\dot{u}\}\, dV = \frac{1}{2}\sum_{k=1}^{N}\int_A\int_{z_{k-1}}^{z_k}\rho_k\{\dot{u}\}^T\{\dot{u}\}\, dz dA\\ U &= \frac{1}{2}\int_V \{\sigma\}^T\{\varepsilon\}\, dV = \sum_{k=1}^{N}\int_A\int_{z_{k-1}}^{z_k}\{\sigma\}_k^T\{\varepsilon\}\, dz dA,\\ W &= \{u\}^T\{f_c\} + \int_{S_1}\{u\}^T\{f_s\}\, dS + \int_V\{u\}^T\{f_v\}\, dV \end{aligned} \tag{12}$$

where N is the number of layers, V_k is the volume and ρ_k is the density of the kth layer. V and S_1 denote the volume and the surface area of the plate, respectively. $\{f_c\}$ denotes the concentrated forces and $\{f_S\}$, $\{f_V\}$ denote the surface and volume forces, respectively. Finally, a dot over a variable represents a time derivative.

Using the displacements relations (1), the strain displacement relations (2) and the constitutive relations (4), the Hamilton's principle (11) can be written as:

$$\begin{aligned}\int_{t_1}^{t_2}\Bigg\{\sum_{k=1}^{N}\left(\int_A\int_{z_{k-1}}^{z_k}\{\delta\varepsilon\}^T\left[\overline{Q}\right]_k\{\varepsilon\}dz dA - \int_A\int_{z_{k-1}}^{z_k}\{\delta\dot{u}\}^T\rho_k\{\dot{u}\}dz dA\right)\\ -\left(\{\delta u\}^T\{f_c\} + \int_A\{\delta u\}^T\{f_s\}\, dA + \int_V\{\delta u\}^T\{f_V\}\, dV\right)\Bigg\}\, dt = 0\end{aligned} \tag{13}$$

Next, the displacements given by Eq. (9) and the strain–nodal displacement relations (10) are substituted in (13) to discretize the variational expression (13). Assembly of the discretized equation for the total number of elements is then implemented and the global mass matrix, stiffness matrix, as well as the displacement and force vectors are derived. The equations of motion of the system can be expressed as follows [27]

$$[M]\{\ddot{d}\} + [K]\{d\} = \{F_m\} \tag{14}$$

where $[M]$, $[K]$, $\{d\}$ and $\{F_m\}$ are the global mass matrix, the global linear stiffness matrix, the global displacement vector and the force vector, respectively. It is noted that the essential boundary conditions are enforced by imposing prescribed values at the corresponding DOF of the discretized domain. Then, in the system of equations of motion, the lines and columns of the prescribed degrees of freedom, as well as the lines of the force vector are eliminated.

3.2. Eigenvalue problem

By setting the force term to zero, and assuming that the plate undergoes a harmonic motion $d = d_0 e^{-i\omega t}$, the generalized governing equation (14) can be used to solve the free vibration problem for the laminated skew plate. In this case, Eq. (14) can be expressed as:

$$[K]\{d_0\} = \lambda [M]\{d_0\} \tag{15}$$

where eigenvalue $\lambda = \omega^2$ and ω is the frequency of natural vibrations. To obtain the numerical solution of the problem, a MATLAB code is developed based on the finite element formulation of the problem. It is noted that the selective integration technique is adopted for the calculation of the stiffness matrix in order to avoid shear locking effect. The present finite element formulation can now be used to solve optimization problems and maximize the fundamental frequency of skew laminates.

4. Effective material properties

The skew plate is a three-phase multiscale laminate reinforced with graphene nanoplatelets and glass or carbon fibres. Effective material properties of the nanocomposite are determined using the Halpin–Tsai model and the rule of mixtures as detailed in [31,32]. First, micromechanical equations are used to determine the effective properties of the (two-phase) graphene-reinforced matrix. Next, using the effective properties of the graphene-reinforced matrix, the properties of the three-phase nanocomposite are computed based on the micromechanical relations given in [33]. It is noted that the present approach of first determining the properties of the two-phase composite and then calculating the overall properties of the three-phase graphene/fibre-reinforced composite, has also been adopted in a number of studies. For example, the micromechanics equations used in [34] for a two-phase fibre-reinforced composite were also applied in [35] to calculate the effective material properties of a three-phase graphene/fibre-reinforced matrix. This approach can also be observed in [36,37].

4.1. Effective material properties of the graphene-reinforced matrix

The effective material properties of graphene-reinforced matrix are determined using the micromechanics equations given in [31,38–40]. Subscripts *GPL*, *M* and *GM* refer to graphene nanoplatelets, the matrix and the graphene-reinforced matrix, respectively. The effective Young's modulus of the graphene-reinforced matrix is calculated using the relation:

$$E_{GM} = \left(\frac{3}{8} \frac{1 + \xi_L \eta_L V_{GPL}}{1 - \eta_L V_{GPL}} + \frac{5}{8} \frac{1 + \xi_w \eta_w V_{GPL}}{1 - \eta_w V_{GPL}} \right) E_M \tag{16}$$

where V_{GPL} is the volume of graphene nanoplatelets and E_M is Young's modulus of the matrix. In Eq. (16), ξ_{L} and ξ_w are given by:

$$\xi_{\mathrm{L}} = 2\frac{l_{GPL}}{h_{GPL}}, \qquad \xi_{\mathrm{w}} = 2\frac{w_{GPL}}{h_{GPL}} \tag{17}$$

where l_{GPL} is the length, w_{GPL} is the width and h_{GPL} is the thickness of the graphene nanoplatelets. The values for η_L and η_w used in Eq. (16) can be determined from the following expressions:

$$\eta_L = \frac{(E_{GPL}/E_M) - 1}{(E_{GPL}/E_M) + \xi_{\mathrm{L}}}, \qquad \eta_w = \frac{(E_{GPL}/E_M) - 1}{(E_{GPL}/E_M) + \xi_w} \tag{18}$$

where E_{GPL} is the Young's modulus of graphene nanoplatelets and E_M is the Young's modulus of the matrix. The volume V_{GPL} of the graphene nanoplatelets can be calculated from the Eq. (19):

$$V_{GPL} = \frac{W_{GPL}}{W_{GPL} + (\rho_{GPL}/\rho_M)(1 - W_{GPL})} \tag{19}$$

where W_{GPL} is the weight fraction of graphene nanoplatelets. The effective shear modulus, Poisson's ratio and density for the graphene-reinforced matrix are given by:

$$G_{GM} = \frac{E_{GM}}{2(1 + \upsilon_{GM})} \tag{20a}$$

$$\upsilon_{GM} = \upsilon_{GPL} V_{GPL} + \upsilon_M (1 - V_{GPL}) \tag{20b}$$

$$\rho_{GM} = \rho_{GPL} V_{GPL} + \rho_M (1 - V_{GPL}) \tag{20c}$$

where ρ_{GPL} and ρ_M represent the mass densities of the graphene nanoplatelets and of the polymer matrix, respectively.

4.2. Effective material properties of the graphene and fibre-reinforced matrix

The effective material properties of the three-phase nanocomposite are determined using the following equations [29,33]:

$$E_{11} = E_{F11} V_F + E_{GM}(1 - V_F) \tag{21}$$

$$E_{22} = E_{GM} \left(\frac{E_{F22} + E_{GM} + (E_{F22} - E_{GM}) V_F}{E_{F22} + E_{GM} - (E_{F22} - E_{GM}) V_F} \right) \tag{22}$$

$$G_{12} = G_{13} = G_{GM} \left(\frac{G_{F12} + G_{GM} + (G_{F12} - G_{GM}) V_F}{G_{F12} + G_{GM} - (G_{F12} - G_{GM}) V_F} \right) \tag{23}$$

$$G_{23} = \frac{E_{22}}{2(1 + \upsilon_{23})} \tag{24}$$

$$\upsilon_{12} = \upsilon_{F12} V_F + \upsilon_{GM}(1 - V_F) \tag{25}$$

$$\upsilon_{23} = \upsilon_{F12} V_F + \upsilon_{GM}(1 - V_F) \left(\frac{1 + \upsilon_{GM} + \frac{\upsilon_{12} E_{GM}}{E_{11}}}{1 - \upsilon_{GM}^2 + \frac{\upsilon_{12} \upsilon_{GM} E_{GM}}{E_{11}}} \right) \tag{26}$$

$$\rho = \rho_F V_F + \rho_{GM}(1 - V_F) \tag{27}$$

In Eqs. (21)–(27), the subscripts F and GM refer to fibres and graphene-reinforced matrix, respectively. V_F and ρ_F denote the fibre volume content and the density, respectively.

5. Optimal design problems

The present study aims to maximize the fundamental frequencies of 45° skew graphene/fibre-reinforced laminates. The design variables are defined as the GPLs and fibre contents of laminate, the layer thicknesses and the fibre orientations. These are among the design variables that crucially affect the mechanical response of laminates, and they are key parameters in industrial applications. A sequence of optimization problems is formulated with the number of design variables increasing from one set to four sets of design variables. This approach makes it possible to evaluate the effectiveness of each set of design variables as compared to one another.

In the first optimization problem, the graphene contents of layers are specified as the design variables taking the layer thicknesses uniform and fibre contents of layers constant. In this case, GPLs are distributed non-uniformly across the thickness. In the second optimization problem, two design variables are specified, namely, the GPLs and fibre contents of each layer, leading to laminates with non-uniformly

distributed reinforcements. In the third design problem, three design variables are the graphene and fibre contents as well as the layer thicknesses leading to laminates with non-uniform layer thicknesses. The last problem involves four design variables, namely, the graphene and the fibre contents, the thickness and the fibre orientation of each layer. As it will become apparent in the numerical results, the chosen order of adding variables leads to a gradual increase of the fundamental frequency, for increasing number of design variables. It is noted that different order of adding variables could also be adopted within the same numerical framework. In such a case, the vibration response may provide additional results, noticing though, that for the case that all design variables are considered (e.g., the four design variables of this article), the same results with the present investigation would be expected. This task is left for future investigation.

The layer thicknesses are denoted by h_k and the number of layers by N. The layer thicknesses are kept constant in the first two optimization problems and the total thickness of the laminate is $Nh = D$.

In the third and fourth optimization problems layer thicknesses h_k are non-uniform and the total laminate thickness is given by $\sum_{k=1}^{N} h_k = D$. The GPL and fibre contents of the kth layer are denoted by V_{GPLk} and V_{Fk}, respectively.

5.1. Optimization problems with one and two design variables

In the first two optimization problems, the layer thicknesses are taken as uniform. Design variables are the GPLs content (Problem 1) and the GPLs and fibre contents (Problem 2). The volume of fibres (Vol_{Fk}) in the kth layer is given by $Vol_{Fk} = abhV_{Fk}$ where h is the layer thickness and V_{Fk} is the fibre volume content of the kth layer. The total volume of fibres in the laminate is then given by summing up the fibre volumes and is given by $Vol_{FT} = \sum_{k=1}^{N} Vol_{Fk} = abh\sum_{k=1}^{N} V_{Fk}$. The maximum fibre volume for the laminate is given by $Vol_{Fmax} = abDV_{Fmax}$ with V_{Fmax} denoting the maximum fibre volume content. The design constraint on the total fibre volume can be expressed as:

$$Vol_{FT} \le Vol_{Fmax} \Rightarrow abh\sum_{k=1}^{N} V_{Fk} \le abDV_{Fmax} \tag{28}$$

Inequality (28) implies that $\frac{h}{D}\sum_{k=1}^{N} V_{Fk} \le V_{Fmax}$. In the present study, the results are given for laminates with 8 layers and in this case, the inequality (28) can be expressed as:

$$\frac{1}{8}\sum_{k=1}^{8} V_{Fk} \le V_{Fmax} \tag{29}$$

Similarly, the constraint on the weight of GPLs can be expressed as:

$$\frac{1}{8}\sum_{k=1}^{8} W_{GPLk} \le W_{GPLmax} \tag{30}$$

where W_{GPLmax} is the total weight of GPLs reinforcement and W_{GPLk} is the weight of GPLs in the kth layer. The optimization problem can be stated as follows:

Maximize the fundamental frequency $\omega\left(V_F, W_{GPL}\right)$ (31a)

subject to the constraints

$$\frac{1}{8}\sum_{k=1}^{8} V_{Fk} \le V_{Fmax} \tag{31b}$$

$$\frac{1}{8}\sum_{k=1}^{8} W_{GPLk} \le W_{GPLmax} \tag{31c}$$

$$W_{GPLk} \ge 0 \tag{31d}$$

$$d_1 \le V_{Fk} \le d_2 \tag{31e}$$

Inequalities (31b) and (31c) are the constraints on the maximum fibre and GPLs contents, respectively. Inequality (31e) limits the minimum and maximum fibre volume content of layers. In the present study, the lower fibre limit is specified as $d_1 = 10\%$ and the upper fibre limit as $d_2 = 60\%$.

An important consideration for optimal design problems is the definition of a criterion that can be used to assess the improvement achieved by optimization as compared to non-optimal designs. Furthermore, the criterion can also be used to compare and assess the contributions of different design parameters for improving the objective function. In the present study, non-optimal solutions correspond to the solutions obtained for laminates with uniform GPLs and fibre distributions across the thickness, that is, $W_{GPLk} = \left(\frac{W_{GPLmax}}{N}\right)$ and $V_{Fk} = \left(\frac{V_{Fmax}}{N}\right)$, for $k = 1$ to N. In order to assess the effectiveness of optimal solutions, a design efficiency factor is introduced. It is defined as the ratio of the maximum fundamental frequency ω_{MAX} corresponding to the optimal design and the frequency ω_0 of the laminate with uniform properties. As such, ω_0 can be described as the reference frequency. In the present case, the reference frequency corresponds to the frequency of a laminate with uniformly distributed graphene and fibre contents across the laminate thickness. Thus, the design efficiency factor is given by:

$$\eta = \frac{\omega_{MAX}\left(V_{Fk}, W_{GPLk}\right)}{\omega_0(V_k, W_k)} \tag{32}$$

where the fibre content V_k and the graphene content W_k of the kth layer of the reference laminate are given by:

$$V_k = \frac{V_{Fmax}}{8}, \quad W_k = \frac{W_{GPLmax}}{8} \quad \text{for } k = 1, 2 \ldots, 8 \tag{33}$$

with V_{Fk} and W_{GPLk} in Eq. (32) determined optimally. For the calculation of the reference frequency ω_0 shown in Eq. (32), a uniform thickness is considered for all layers and a symmetric stacking sequence $[90/0/90/0]_s$ is adopted.

5.2. Optimization problems with three and four design variables

Optimization problems with three and four design variables and non-uniform layer thicknesses are formulated next. In this case, in addition to the contents of fibres and GPLs in each layer, the layer thicknesses and the fibre angles are also determined optimally. For these design problems, non-uniform layer thickness of the kth layer is denoted as h_k and the fibre volume as $Vol_{Fk} = abh_kV_{Fk}$. The total fibre volume of the laminate is $Vol_{FT} = \sum_{k=1}^{N} Vol_{Fk} = ab\sum_{k=1}^{N} h_kV_{Fk}$. The constraint on the total volume of fibres is defined as:

$$Vol_{FT} \le Vol_{Fmax} \Rightarrow ab\sum_{k=1}^{N} h_kV_{Fk} \le abDV_{Fmax} \tag{34}$$

which leads to the constraint:

$$\frac{1}{D}\sum_{k=1}^{N} h_kV_{Fk} \le V_{Fmax} \tag{35}$$

Similarly, the constraint on the total graphene weight is

$$\frac{1}{D}\sum_{k=1}^{N} h_kW_{GPLk} \le W_{GPLmax} \tag{36}$$

Layer thicknesses are subject to the constraint:

$$\sum_{k=1}^{N} \frac{h_k}{D} = 1 \tag{37}$$

For an 8-layered laminate, the optimal design problem with four design variables can be expressed as:

Maximize the fundamental frequency $\omega\left(V_{Fk}, W_{GPLk}, \frac{h_k}{D}, \theta_k\right)$ (38a)

subject to:

$$\frac{1}{D}\sum_{k=1}^{8} h_k V_{Fk} \le V_{Fmax} \tag{38b}$$

$$\frac{1}{D}\sum_{k=1}^{8} h_k W_{GPLk} \le W_{GPLmax} \tag{38c}$$

$$W_{GPLk} \ge 0 \tag{38d}$$

$$d_1 \le V_{Fk} \le d_2 \tag{38e}$$

$$-90^\circ \le \theta_k \le 90^\circ \tag{38f}$$

$$\sum_{k=1}^{8} \frac{h_k}{D} = 1 \tag{38g}$$

The inequality (38f) limits the fibre orientation of the kth layer, θ_k. The design efficiency factor for this case, which involves four design variables, is given by:

$$\eta = \frac{\omega_{MAX}\left(V_{Fk}, W_{GPLk}, \frac{h_k}{D}, \theta_k\right)}{\omega_0(V_k, W_k, \frac{h}{D}, \theta_0)} \tag{39}$$

with V_{Fk}, W_{GPLk}, h_k/D and θ_k to be determined optimally. For the calculation of the reference frequency ω_0 shown in Eq. (39), V_k and W_k are given by Eq. (33), a uniform thickness is considered for all layers and a symmetric stacking sequence $[90/0/90/0]_s$ is adopted.

5.3. Optimization algorithm

For the numerical solution of the optimal design problems, Sequential Quadratic Programming Algorithm (SQP) is implemented. SQP generates a sequence of steps by solving quadratic sub-problems for nonlinearly constrained problems [41–43]. At each iteration, the algorithm calculates an approximation of the Hessian of the Lagrangian function using a quasi-Newton updating method which searches for zero values, local maxima and local minima of the function. This is then adopted to create a Quadratic Programming sub-problem with the solution used to define a search direction. More details for the SQP algorithm can be found in [41]. The solution is implemented using MATLAB [44].

6. Verification of the optimization code

The finite element formulation and the optimization scheme are verified using the results available in the literature and ABAQUS commercial finite element software. First, the frequencies obtained in the present work are compared with skew plate frequencies available in the literature. The first four eigenfrequencies calculated by the proposed finite element formulation are compared with the frequencies given in [8], using skew angles of $\alpha = 30^\circ$ and $\alpha = 45^\circ$ for SSSS and CCCC boundary conditions. Material and geometric properties are $E_{11}/E_{22} = 40, G_{12} = G_{13} = 0.6E_2, G_{23} = 0.5E_2, \nu_{12} = \nu_{13} = \nu_{23} = 0.25, a/D = 10$ [8]. The non-dimensional frequency is given by $\Omega = (\omega a^2/\pi^2 D)\sqrt{\rho/E_2}$. The results are presented in Tables 1 and 2, for two stacking sequences of $\alpha = 30^\circ$ and $\alpha = 45^\circ$. The comparison indicates that frequencies obtained by the present approach are close to those in [8].

To further verify the results in the present article, frequencies are compared with those given in [45] for different skew angles. Material and geometric properties are taken as $E_{11}/E_{22} = 40, G_{12} = 0.6E_2, G_{13} = G_{23} = 0.5E_2, \nu_{12} = \nu_{13} = \nu_{23} = 0.25, a/D = 10$ [45].

Results presented in Tables 3 and 4 indicate that the frequencies obtained by the present approach and the ones given in [45] are quite close.

A further comparison is given between the frequencies obtained by the present approach and the ones given in [46] for cantilever skew plates. The material properties are taken as $E_{11} = E_{22}, G_{12} = E_{11}/(2(1+\upsilon))$, $G_{13} = G_{23} = G_{12}$, with $E_{11} = 71.02$ GPa, $\upsilon = 0.333$. In Table 5, the results of the comparison are presented for different aspect and length-to-thickness ratios. It is observed that the frequencies of the two approaches are quite close for different skew angles.

To verify the overall optimization scheme, a model of the two-layered skew cantilever laminate with uniformly distributed graphene nanoplatelets, fibre reinforcements and layer thicknesses is developed using commercial finite element software. A 10 × 14 mesh size is used and shell elements are adopted. The skew angle for this case is specified as 45°. To compare with the optimization results, a different stacking sequence is adopted at each finite element simulation and the corresponding frequency is computed. Subsequently, an optimization problem is formulated and solved using the proposed optimization method with fibre angles specified as the only design variables. This process aims to compare the optimal frequency and fibre orientations obtained from the optimization with the maximum frequency and the corresponding stacking sequence calculated using the commercial finite element software.

Table 1
Fundamental frequencies $\Omega = (\omega a^2/\pi^2 D)\sqrt{\rho/E_2}$ of 5-layered skew laminates with stacking sequence [90/0/90/0/90], $a/D = 10$, $a/b = 1$.

Skew angle	Mode	SSSS		CCCC	
		Present work (mesh 12 × 12)	Ref. [8]	Present work (mesh 12 × 12)	Ref. [8]
30	1	2.0848	2.0911	2.8388	2.8003
	2	3.6112	3.5138	4.1801	4.0576
	3	4.7697	4.7002	5.1229	5.0306
	4	5.0427	4.8869	5.4646	5.3010
45	1	2.8410	2.8829	3.5274	3.4745
	2	4.3390	4.2841	4.8950	4.7408
	3	5.8240	5.5876	6.1907	5.9583
	4	6.2147	6.1920	6.5084	6.3817

Table 2
Fundamental frequencies $\Omega = (\omega a^2/\pi^2 D)\sqrt{\rho/E_2}$ of 5-layered skew laminates with stacking sequence [45/−45/45/−45/45], $a/D = 10$, $a/b = 1$.

Skew angle	Mode	SSSS		CCCC	
		Present work (mesh 12 × 12)	Ref. [8]	Present work (mesh 12 × 12)	Ref. [8]
30	1	2.1039	2.0018	2.7137	2.6641
	2	3.7737	3.6276	4.2492	4.1408
	3	4.4619	4.2875	4.8365	4.7411
	4	5.281	5.0723	5.6414	5.5027
45	1	2.5616	2.4796	3.4126	3.3529
	2	4.4007	4.2221	4.9539	4.8122
	3	5.7859	5.5867	6.1886	6.0713
	4	5.8596	5.6013	6.3145	6.1108

Table 3
Fundamental frequency $\Omega = (\omega a^2/\pi^2 D)\sqrt{\rho/E_2}$ of 5-layered skew laminates with stacking sequence [90/0/90/0/90], $a/D = 10$, $a/b = 1$.

Skew angle	SSSS		CCCC	
	Present work (mesh 12 × 12)	Ref. [45]	Present work (mesh 12 × 12)	Ref. [45]
15	1.6892	1.6874	2.4323	2.4750
30	2.0348	2.0884	2.7327	2.7922
45	2.7525	2.8932	3.3793	3.4739

Table 4
Fundamental frequency $\Omega = (\omega a^2/\pi^2 D)\sqrt{\rho/E_2}$ of 4-layered skew laminates with stacking sequence [45/−45/45/−45], $a/D = 10$, $a/b = 1$.

Skew angle	SSSS		CCCC	
	Present work (mesh 12 × 12)	Ref. [45]	Present work (mesh 12 × 12)	Ref. [45]
15	1.9653	1.9366	2.3752	2.4007
30	2.1482	2.1196	2.7024	2.7418
45	2.6237	2.6752	3.3759	3.4434

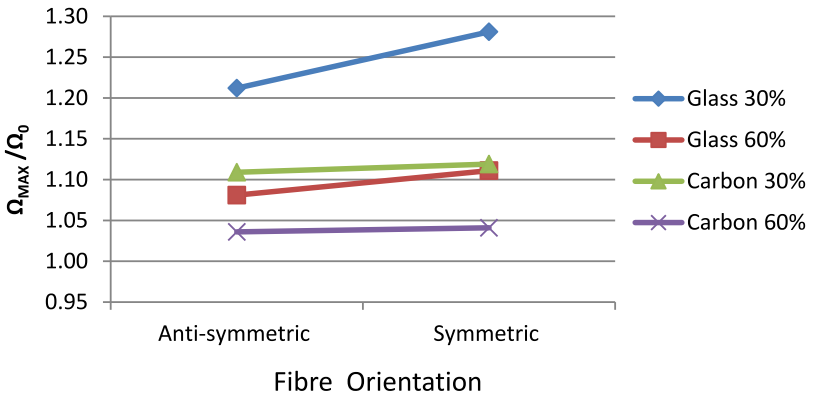

Fig. 3. Design efficiencies of anti-symmetric and symmetric laminates with GPLs content as the single design variable.

Table 5
Fundamental frequencies (Hz) of cantilever thin skew plates.

Skew angle	Aspect ratio a/b	Length-to-thickness ratio a/D	Mode	CFFF	
				Present work (mesh 15 × 15)	Ref. [46]
15	2.80	143	1	42.240	42.1970
			2	235.200	234.280
			3	278.146	275.620
			4	704.614	690.730
30	2.43	138.5	1	47.5120	47.441
			2	234.410	233.320
			3	330.610	327.060
			4	687.360	675.860
45	1.89	138	1	53.631	53.450
			2	223.690	222.400
			3	394.000	387.980
			4	629.730	618.940
60	1.35	138.5	1	65.400	64.688
			2	235.650	233.410
			3	462.590	452.010
			4	677.100	657.240

Table 6
Properties of constituent materials.

Material	E_{11} (GPa)	E_{22} (GPa)	G_{12} (GPa)	υ_{12}	Density (kg/m^3)
GPLs	1010	1010	$E_{11}/2(1+\nu)$	0.186	1060
Matrix	3	3	$E_{11}/2(1+\nu)$	0.34	1200
Carbon fibres	263	19	27.60	0.20	1750
Glass fibres	72.4	72.4	$E_{11}/2(1+\nu)$	0.20	2400

A non-dimensional fundamental frequency Ω is defined and used for the present results, as well as in the subsequent sections of the article:

$$\Omega = \omega D\sqrt{\frac{\rho_M}{E_M}} \tag{40}$$

with ρ_M and E_M representing the density and the Young's modulus of the matrix. The material properties used in the numerical results are given in Table 6. Dimensions of GPLs used in the present and subsequent sections are $l_{GPL} = 2.5$ μm, $w_{GPL} = 1.5$ μm, and $h_{GPL} = 1.5$ nm. The weight of GPLs is specified as 1% and the fibre volume content as 50%. The results of this comparison are given in Table 7.

Results obtained using the commercial software package show that the stacking sequence $[0°, 0°]$ produces the maximum frequency which is equal to 0.00364. The present optimization scheme gives a maximum frequency of 0.0037 with fibre orientations of $[-0.28°, 0.28°]$. Thus, both the solution produced by the commercial finite element software and the one obtained by the proposed MATLAB optimization code lead to almost identical results for the optimal frequency and the fibre orientations.

7. Results and discussions

7.1. Optimization using the graphene content as the single design variable

In the present case, GPLs distribution across the thickness is the only design variable. Layer thicknesses and fibre distributions are defined as uniform with the results given for symmetric and anti-symmetric laminates. Numerical results are given for the fibre volume contents of 30% and 60% in Table 8. The frequency of the optimal laminates is indicated in non-dimensional form in Eq. (40) as Ω. The non-dimensional frequency Ω_0 of the reference laminate is determined by substituting ω_0 as defined at the end of Section 5.1, into the Eq. (40). Design efficiency for this case is given by $\eta = \frac{\Omega}{\Omega_0}$ which is the same as the one defined in Section 5.1 by Eq. (32).

Table 8 indicates that the distribution of the GPLs across the thickness tends to be higher in the outer layers with the inner layers having zero GPLs content. This is due to the outer layers contributing more to the laminate stiffness as compared to the middle layers. It is noted that a significant increase in the fundamental frequency is observed with the GPLs distributed optimally as compared to the laminates with uniformly distributed GPLs. A maximum increase of 28.1% is observed for the symmetric laminates having a glass fibre content of 30%. The corresponding increase for the anti-symmetric laminates is 21.2%. Concerning the laminates with 30% carbon fibre content, the fundamental frequency increases by 11.9% for the symmetric and 10.9% for the anti-symmetric cases. In the case of laminates with 60% glass or carbon fibre contents, a lower percent of increase in the frequency is observed. The increase in the fundamental frequency of laminates with optimal GPLs distributions is shown in Fig. 3.

Table 7
Comparison of the optimal non-dimensional frequencies Ω with those obtained from the commercial finite element software for GPLs/glass fibre skew plates with $D/a = 0.03$, $W_{GPL} = 0.01$, $V_F = 0.50$, $a/b = 0.71$ and skew angle $\alpha = 45°$.

Solution obtained by the commercial finite element software			Solution obtained by the proposed optimization code	
Case	Stacking sequence	Non-dimensional frequency	Optimal stacking sequence	Optimal non-dimensional frequency
1	**[0,0]**	**0.00364**	[−0.28, 0.28]	0.0037
2	[30,0]	0.00356		
3	[45,0]	0.00336		
4	[60,0]	0.00332		
5	[90,0]	0.00333		
6	[0,30]	0.00344		
7	[30,30]	0.00328		
8	[45,30]	0.00320		
9	[60,30]	0.00317		
10	[90,30]	0.00318		
11	[0,45]	0.00336		
12	[30,45]	0.00320		
13	[45,45]	0.00313		
14	[60,45]	0.00310		
15	[90,45]	0.00311		
16	[0,60]	0.00332		
17	[30,60]	0.00317		
18	[45,60]	0.00310		
19	[60,60]	0.00306		
20	[90,60]	0.00307		
21	[0,90]	0.00333		
22	[30,90]	0.00318		
23	[45,90]	0.00311		
24	[60,90]	0.00307		
25	[90,90]	0.00309		

Table 8
Optimal fundamental frequencies of an 8-layered cantilever skew laminates having the design variable W_{GPL} with $W_{GPLmax} = 0.0125$, $D/a = 0.03$, $h/D = 0.125$, $a/b = 0.71$ and skew angle $\alpha = 45°$.

Stacking sequence	Fibre content	Optimal W_{GPL} per layer	Ω	Ω_0	$\eta = \frac{\Omega}{\Omega_0}$
$[90/0/90/0]_{\text{anti-s}}$	Glass 30%	$[0.050/0.0/0.0/0.0]_{\text{anti-s}}$	0.0040	0.0033	1.212
	Glass 60%	$[0.039/0.011/0.0/0.0]_{\text{anti-s}}$	0.0040	0.0037	1.081
	Carbon 30%	$[0.050/0.0/0.0/0.0]_{\text{anti-s}}$	0.0051	0.0046	1.109
	Carbon 60%	$[0.041/0.009/0.0/0.0]_{\text{anti-s}}$	0.0057	0.0055	1.036
$[90/0/90/0]_{\text{s}}$	Glass 30%	$[0.050/0.0/0.0/0.0]_{\text{s}}$	0.0041	0.0032	1.281
	Glass 60%	$[0.048/0.002/0.001/0.0]_{\text{s}}$	0.0040	0.0036	1.111
	Carbon 30%	$[0.050/0.0/0.0/0.0]_{\text{s}}$	0.0047	0.0042	1.119
	Carbon 60%	$[0.041/0.009/0.001/0.0]_{\text{s}}$	0.0051	0.0049	1.041

The highest fundamental frequency is obtained for the anti-symmetric case for laminates with a 60% carbon fibre content as shown in Table 8. An increase of 42.5% in the frequency is observed for this case as compared to the frequency of the graphene and glass fibre-reinforced anti-symmetric laminates with 60% fibre content. Table 8 indicates that graphene–glass fibre-reinforced laminates with 30% and 60% fibre contents have the same frequency for the anti-symmetric case. For the symmetric case, laminates with 30% glass fibre content have a slightly higher frequency than those with 60% glass fibre content. Thus, higher glass fibre content has a minor effect on the fundamental frequency for cross-ply laminates.

The design efficiencies of the graphene–glass fibre-reinforced laminates with optimal GPL distribution across the thickness are investigated in Fig. 4. Glass fibre reinforcement is uniformly distributed with a 30% fibre content. Results are given for symmetric and anti-symmetric laminates. It is observed that the effect of the stacking sequence on the design efficiency depends on the type of stacking sequence with anti-symmetric laminates having higher design efficiencies up to $[50/40/50/40]_{\text{anti-s}}$ stacking sequence. Symmetric laminates have higher design efficiencies for the stacking sequences $[75/30/75/30]_{\text{s}}$ and $[90/0/90/0]_{\text{s}}$ indicating that design efficiencies depend on the type of laminate.

Maximum fundamental frequencies are plotted against GPLs weight contents in Fig. 5 for the symmetric stacking sequences and in Fig. 6 for the anti-symmetric stacking sequences. The design variable in Figs. 5 and 6 is the optimal distribution of GPLs across the thickness with fibres distributed uniformly. Results are given up to a graphene weight of 10% to observe the effect of high graphene content on the frequency and determine the cross-over points.

Fig. 5 shows that the frequencies of the symmetric graphene–glass fibre-reinforced laminates are higher for 60% fibre content up to a value of about 1% graphene content. Afterwards, laminates with 30% fibre content have higher frequencies than those with 60% glass fibre content. A similar trend is observed for the anti-symmetric graphene–glass fibre laminates as shown in Fig. 6.

In the case of carbon fibre-reinforced laminates, the same phenomenon is observed for both the symmetric and the anti-symmetric cases but for a higher graphene weight of about 3%. These results indicate that higher fibre content exceeding a certain value (cross-over points) leads to diminishing returns and not cost-effective designs for skew laminates. In the case of 60% fibre reinforcements, a significant drop is observed in the slope of the curves as shown in Figs. 5 and 6 after the cross-over points which highlights this comment.

7.2. Optimization using GPLs and fibre distributions as design variables

The next optimization problem introduces two design variables, namely the GPLs and the fibre contents. Layer thicknesses are specified as uniform and the results are shown in Table 9.

Table 9 indicates that optimization leads to higher GPL and fibre contents in the outer layers as expected. Similar to the previous case of optimization using only the GPL distribution as the design variable,

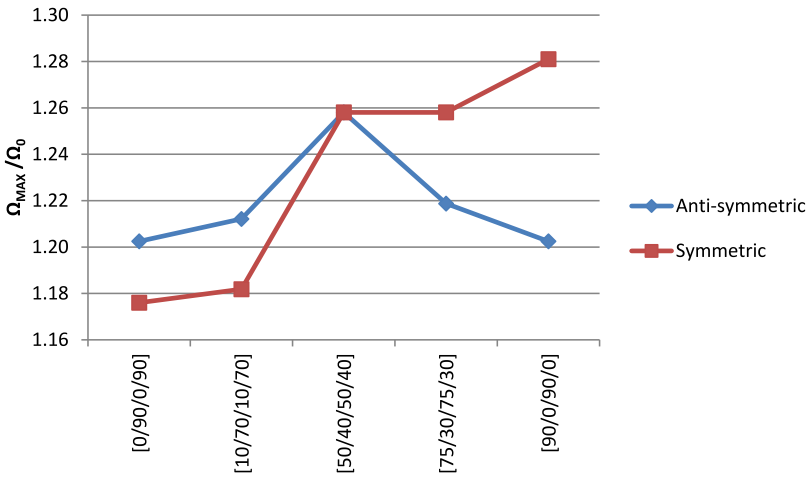

Fig. 4. Design efficiencies for anti-symmetric and symmetric laminates with GPLs content as the single design variable and 30% uniform glass fibre distribution.

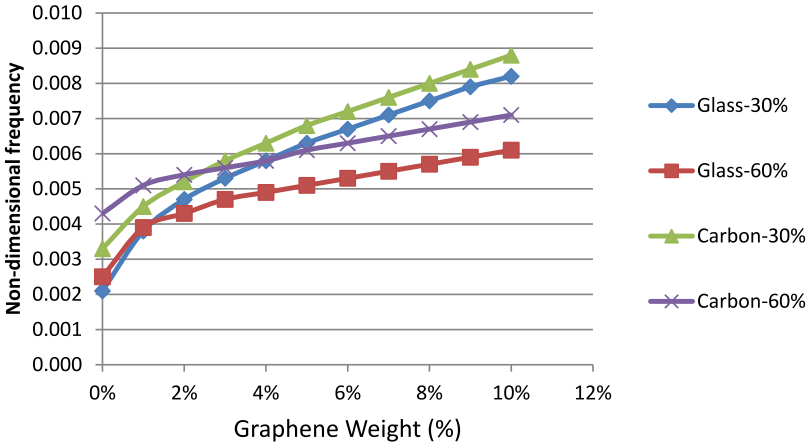

Fig. 5. Fundamental frequency vs. GPLs content for laminates with symmetric stacking sequence $[90/0/90/0]_s$, $D/a = 0.03$, $h/D = 0.125$, $a/b = 0.71$ and skew angle $\alpha = 45°$.

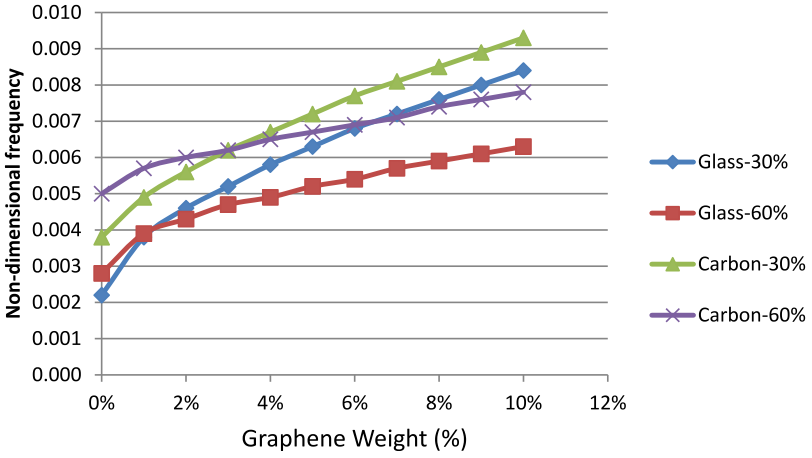

Fig. 6. Fundamental frequency vs. GPLs content for laminates with anti-symmetric stacking sequence $[90/0/90/0]_{anti\text{-}s}$, $D/a = 0.03$, $h/D = 0.125$, $a/b = 0.71$ and skew angle $\alpha = 45°$.

glass fibre reinforcement leads to higher design efficiencies as compared to the carbon fibre reinforcement. For the symmetric laminates, design efficiency is 34% and for the anti-symmetric laminates 27% in the case of glass fibre reinforcements. Both these values are higher as compared to carbon fibre-reinforced laminates as shown in Table 9. Compared to carbon fibres, lower material properties in the case of glass fibres, resulting in a lower laminate stiffness, leads to GPL reinforcements being more effective for graphene–glass fibre laminates. It is noted that this result applies to design efficiencies, and not the maximum frequencies which are higher in the case of carbon fibre reinforcements as expected.

A comparison between Tables 8 and 9 indicates the effect of increasing the number of design variables on the fundamental frequency. With carbon fibre reinforcement, frequency increases by 9.8% for anti-symmetric and by 17% for symmetric stacking sequence. In the case of glass fibre reinforcement, the corresponding frequency increase is

Table 9
Fundamental frequencies of 8-layered laminates with two design variables, namely, GPLs and fibre distributions across the thickness with $W_{GPLmax} = 0.0125$, $V_{Fmax} = 0.30$, $D/a = 0.03$, $h/D = 0.125$, $a/b = 0.71$ and skew angle $\alpha = 45°$.

Stacking sequence	Fibres	Optimal W_{GPL} per layer	Optimal V_F per layer	Ω	Ω_0	$\eta = \frac{\Omega}{\Omega_0}$
$[90/0/90/0]_{anti\text{-}s}$	Glass	$[0.037/0.013/0.0/0.0]_{anti\text{-}s}$	$[0.60/0.40/0.10/0.10]_{anti\text{-}s}$	0.0042	0.0033	1.273
	Carbon	$[0.047/0.004/0.0/0.0]_{anti\text{-}s}$	$[0.43/0.57/0.10/0.10]_{anti\text{-}s}$	0.0056	0.0046	1.217
$[90/0/90/0]_s$	Glass	$[0.050/0.0/0.0/0.0]_s$	$[0.40/0.60/0.10/0.10]_s$	0.0043	0.0032	1.344
	Carbon	$[0.050/0.0/0.0/0.0]_s$	$[0.10/0.60/0.40/0.10]_s$	0.0055	0.0042	1.310

Table 10
Fundamental frequency of an 8-layered skew laminate with zero graphene content and the single design variable V_F subject to $V_{Fmax} = 0.30$ with $D/a = 0.03$, $h/D = 0.125$, $a/b = 0.71$ and skew angle $\alpha = 45°$.

Stacking sequence	Fibres	Optimal V_F per layer	Ω	Ω_{02}	$\eta_2 = \frac{\Omega}{\Omega_{02}}$	$\eta = \frac{\Omega}{\Omega_0}$
$[90/0/90/0]_{anti\text{-}s}$	Glass	$[0.60/0.40/0.10/0.10]_{anti\text{-}s}$	0.0027	0.0022	1.227	0.818
	Carbon	$[0.54/0.46/0.10/0.10]_{anti\text{-}s}$	0.0046	0.0038	1.211	1.000
$[90/0/90/0]_s$	Glass	$[0.40/0.60/0.10/0.10]_s$	0.0025	0.0021	1.190	0.781
	Carbon	$[0.10/0.60/0.40/0.10]_s$	0.0043	0.0033	1.303	1.024

5% for anti-symmetric and 4.9% for symmetric stacking sequences. These results indicate that a cost-effective design can be achieved using less fibre reinforcement if both graphene and fibres are distributed optimally across the thickness.

To assess the effect of GPLs reinforcement on optimal design, graphene content is set to zero and optimization is performed using the fibre reinforcement as the only design variable. The results are given in Table 10 for both anti-symmetric and symmetric cases.

Two design efficiencies are shown in Table 10, namely, $\eta_2 = \frac{\Omega}{\Omega_{02}}$, and $\eta = \frac{\Omega}{\Omega_0}$. The design efficiency η_2 is computed as the ratio of the maximum frequency Ω and the reference frequency Ω_{02} corresponding to a laminate with zero graphene content. This index can be used to evaluate the increase in the fundamental frequency of the laminate with non-uniform (optimal) fibre distribution only as compared to the frequency of the reference laminate with uniform fibre distribution across the thickness. In addition, η is calculated using the reference frequency Ω_0, which corresponds to the frequency of a laminate with uniform graphene content of 1.25% per layer. This index will be used to compare the efficiencies of the optimal two-phase fibre-reinforced composite laminates (only fibre reinforcement, Table 10) and the efficiencies of the optimal three-phase graphene/fibre-reinforced laminates (Table 9).

Noting the values η_2 of the design efficiency, it is observed that a significant increase of η_2 from 19% to 30% is observed for the two-phase fibre-reinforced laminate with optimal (non-uniform) fibre distribution across the laminate thickness as compared to the frequency corresponding to the laminate with uniform fibre distribution.

To investigate the impact of introducing graphene reinforcement on the frequency, a comparison of the results presented in Table 10 (zero graphene, optimal distribution of fibres) and Table 9 (optimal distribution of both graphene and fibres) is made. For the anti-symmetric laminate with non-zero graphene and glass fibre reinforcement, a design efficiency of 1.273 is obtained in Table 9, indicating an increase of 27.3% of the frequency as compared to the reference plate. For the same fibre type and orientation, but for zero graphene content (Table 10), the design efficiency η is 0.818 which indicates a decrease of $1.000 - 0.818 = 0.182$ or 18.2% in the fundamental frequency as compared to the reference frequency. For this case, the overall increase of the fundamental frequency of the laminate with non-zero graphene content is equal to 27.3%+18.2%=45.5% as shown in Table 11 in comparison to the laminate with zero graphene. This is a substantial improvement of the frequency which is due to adding a small graphene content as reinforcement.

As shown in Table 11, an even higher increase of 56.3% is obtained for the symmetric glass fibre/graphene-reinforced laminate. For anti-symmetric and symmetric carbon fibre/graphene-reinforced laminates, the increases of the fundamental frequency are equal to 21.7% and 28.6%, respectively, as compared to the frequencies of the optimal two-phase fibre-reinforced laminates.

7.3. Optimization with three and four design variables and non-uniform layer thicknesses

Next, non-uniform layer thicknesses and fibre angles are introduced as additional design variables, leading to optimization with three and four design variables. These are graphene and fibre contents, the layer thicknesses and the fibre angles. Results with three design variables and predefined stacking sequences are given in Table 12.

Table 12 indicates that higher graphene and fibre reinforcements are assigned to outer layers as expected. Furthermore, two outer layers have lower thicknesses as compared to the inner layers for the anti-symmetric laminates. In the case of symmetric laminates, only the surface layer has a lower thickness with the other layers having the same thicknesses. The increase in the fundamental frequency, as compared to the reference frequency, is 30.3% and 23.9% for the anti-symmetric case with glass and carbon fibre reinforcements, respectively. For the symmetric laminate, the increases are 46.9% and 54.8%, and thus, significantly higher than the anti-symmetric case. A comparison with the laminates with uniform layer thicknesses (Table 9), indicates that in the case of non-uniform layer thicknesses (Table 12), an increase in the fundamental frequency, with respect to the reference frequency, occurs. For the anti-symmetric case, this is equal to 3% and 2.2% for glass and carbon fibre reinforcements. For the symmetric laminates with non-uniform layer thicknesses, the increase in the fundamental frequency is 12.5% and 23.8% for glass and carbon fibre reinforcements, respectively.

The fourth optimization problem involves GPLs and fibre contents, layer thicknesses and fibre angles as the design parameters, with the results shown in Table 13.

The increase in the fundamental frequency (compared to reference frequency) of anti-symmetric laminates is 45.5% for glass fibre and 52.2% for carbon fibre reinforcements. For the symmetric laminate, the increase is 46.9% for glass fibre and 64.3% for carbon fibre reinforcements. The same increase was observed for the symmetric laminates with glass fibre reinforcement and predefined stacking sequence, as shown in Table 12. Therefore, the stacking sequence $[90/0/90/0]_s$, which was used in Table 12, is the optimal one.

In the case of laminates with four design variables (Table 13) involving glass and carbon fibres (anti-symmetric laminate) and carbon fibres (symmetric laminate), the increases in the fundamental frequencies (comparing to reference frequency) are higher by 15.2%, 28.3%, and 9.5% as compared to the case with three design variables (Table 12).

The improvement in the frequencies is due to including the fibre angles in the optimization process. It is noted that for both anti-symmetric and symmetric cases, higher frequency and higher design efficiency are observed for carbon fibre-reinforced laminates as compared to the glass fibre-reinforced ones.

Table 11
Comparison between the maximum and the reference frequencies for the results shown in Table 9 (non-zero, optimal graphene/fibre distribution) and Table 10 (zero graphene, optimal fibre distribution).

	Stacking sequence	Fibre type	Maximum frequency Ω	Reference frequency Ω_0	$\eta = \frac{\Omega}{\Omega_0}$	$\frac{\Omega-\Omega_0}{\Omega_0}$ (%)
Optimal graphene distribution	$[90/0/90/0]_{anti\text{-}s}$	Glass	0.0042	0.0033	1.273	27.30%
		Carbon	0.0056	0.0046	1.217	21.70%
	$[90/0/90/0]_s$	Glass	0.0043	0.0032	1.344	34.40%
		Carbon	0.0055	0.0042	1.310	31.00%
Zero graphene	$[90/0/90/0]_{anti\text{-}s}$	Glass	0.0027	0.0033	0.818	−18.20%
		Carbon	0.0046	0.0046	1.000	0
	$[90/0/90/0]_s$	Glass	0.0025	0.0032	0.781	−21.90%
		Carbon	0.0043	0.0042	1.024	2.40%

Table 12
Fundamental frequencies of 8-layered skew laminates with three design variables (GPLs and fibre contents, thickness ratios) and with $W_{GPLmax} = 0.0125$, $V_{Fmax} = 0.30$, $D/a = 0.03$, $a/b = 0.71$ and skew angle $\alpha = 45°$.

Stacking sequence	Fibres	Optimal W_{GPL} per layer	Optimal V_F per layer	h/D	Ω	Ω_0	$\eta = \frac{\Omega}{\Omega_0}$
$[90/0/90/0]_{anti\text{-}s}$	Glass	$[0.046/0.019/0.0/0.0]_{anti\text{-}s}$	$[0.60/0.60/0.10/0.10]_{anti\text{-}s}$	$[0.09/0.11/0.15/0.15]_{anti\text{-}s}$	0.0043	0.0033	1.303
	Carbon	$[0.054/0.016/0.0/0.0]_{anti\text{-}s}$	$[0.60/0.60/0.10/0.10]_{anti\text{-}s}$	$[0.08/0.12/0.15/0.15]_{anti\text{-}s}$	0.0057	0.0046	1.239
$[90/0/90/0]_s$	Glass	$[0.127/0.0/0.0/0.0]_s$	$[0.10/0.60/0.27/0.10]_s$	$[0.05/0.15/0.15/0.15]_s$	0.0047	0.0032	1.469
	Carbon	$[0.127/0.0/0.0/0.0]_s$	$[0.10/0.60/0.27/0.10]_s$	$[0.05/0.15/0.15/0.15]_s$	0.0065	0.0042	1.548

Table 13
Fundamental frequencies of 8-layered skew laminates with four design variables (GPLs and fibre contents, thickness ratios, fibre angles) and with $W_{GPLmax} = 0.0125$, $V_{Fmax} = 0.30$, $D/a = 0.03$, $a/b = 0.71$ and skew angle $\alpha = 45°$.

Fibres	Optimal W_{GPL} per layer	Optimal V_F per layer	h/D	Optimal fibre angles	Ω	Ω_0	$\eta = \frac{\Omega}{\Omega_0}$
Glass	$[0.141/0.0/0.0/0.0]_{anti\text{-}s}$	$[0.10/0.60/0.27/0.10]_{anti\text{-}s}$	$[0.05/0.15/0.15/0.15]_{anti\text{-}s}$	$[45/-8/-8/29]_{anti\text{-}s}$	0.0048	0.0033	1.455
Carbon	$[0.141/0.0/0.0/0.0]_{anti\text{-}s}$	$[0.10/0.60/0.27/0.10]_{anti\text{-}s}$	$[0.05/0.15/0.15/0.15]_{anti\text{-}s}$	$[-9/-5/-6/-25]_{anti\text{-}s}$	0.0070	0.0046	1.522
Glass	$[0.127/0.0/0.0/0.0]_s$	$[0.10/0.60/0.27/0.10]_s$	$[0.05/0.15/0.15/0.15]_s$	$[90/0/90/0]_s$	0.0047	0.0032	1.469
Carbon	$[0.027/0.045/0.0/0.0]_s$	$[0.60/0.10/0.27/0.10]_s$	$[0.15/0.05/0.15/0.15]_s$	$[-6/50/-18/88]_s$	0.0069	0.0042	1.643

Table 14
Fundamental frequencies of 8-layered skew ($a/b = 0.71$) and rectangular ($a/b = 1$) laminates with the design variable W_{GPL} and with $W_{GPLmax} = 0.0125$, $D/a = 0.03$, $h/D = 0.125$.

Symmetric fibre orientation $[90°/0°/90°/0°]_s$						
Fibre type	Laminate type	W_{GPL}	Ω	Increase (%)	Ω_0	$\eta = \frac{\Omega}{\Omega_0}$
Glass 30%	Rectangular (0°)	$[0.057/0.0/0.0/0.0]_s$	0.0031	–	0.0024	1.292
	45° Skew	$[0.050/0/0/0]_s$	0.0041	32%	0.0032	1.281
Carbon 30%	Rectangular (0°)	$[0.057/0.0/0.0/0.0]_s$	0.0036	–	0.0032	1.125
	45° Skew	$[0.05/0/0/0]_s$	0.0047	31%	0.0042	1.119

Table 15
Fundamental frequencies of 8-layered skew ($a/b = 0.71$) and rectangular ($a/b = 1$) laminates with two design variables (GPLs and fibre contents) and with $W_{GPLmax} = 0.0125$, $V_{Fmax} = 0.30$, with $D/a = 0.03$, $h/D = 0.125$.

Symmetric fibre orientation $[90°/0°/90°/0°]_s$							
Fibre type	Laminate type	W_{GPL}	V_F	Ω	Increase (%)	Ω_0	$\eta = \frac{\Omega}{\Omega_0}$
Glass	Rectangular (0°)	$[0.0565/0.0/0.0/0.0]_s$	$[0.4/0.6/0.1/0.1]_s$	0.0033	–	0.0024	1.375
	45° Skew	$[0.050/0.0/0.0/0.0]_s$	$[0.4/0.6/0.1/0.1]_s$	0.0043	30%	0.0032	1.344
Carbon	Rectangular (0°)	$[0.0565/0.0/0.0/0.0]_s$	$[0.1/0.6/0.1/0.4]_s$	0.0045	–	0.0032	1.406
	45° Skew	$[0.050/0.0/0.0/0.0]_s$	$[0.1/0.6/0.4/0.1]_s$	0.0055	22%	0.0042	1.310

7.4. Comparison of the optimal designs of rectangular and skew laminates

In this section a comparison of the frequencies of the skew and rectangular plates is presented with both plates being cantilevers. Results are given for one, two, three and four design variables. The fundamental frequencies for these cases are shown in Tables 14 to 17 with the number of design variables increasing from one to four.

Results indicate that the fundamental frequencies of the skew laminates are higher than those of the rectangular laminates for both glass and carbon fibre reinforcements. As observed in Tables 14 to 17, increases are 32%, 30%, 31% and 47% for laminates with glass fibre reinforcement with the increasing number of variables. In the case of carbon fibre reinforcement, the increases in the fundamental frequencies of the skew laminates as compared to the rectangular laminates are 31%, 22%, 18% and 17% for laminates with one, two, three and four design variables, respectively. These results agree with the results given in the Refs. [5–8] where it was noted that the increase of the skew angle increases the fundamental frequency.

Even though the fundamental frequencies of skew plates are higher, their design efficiencies are lower compared to the rectangular plates as shown in Tables 14–17. However, in the case of the skew plate with glass fibre reinforcement and with four design variables, design efficiency is higher than the rectangular plate as shown in Table 17. Since higher design efficiencies are derived for most of the rectangular plates as compared to the skew plates, the fundamental frequency increases are higher for the rectangular plates as compared to the skew plates. Thus, optimal, non-uniform graphene and fibre distributions along the thickness is more effective for rectangular plates. The highest design efficiency is obtained for the rectangular plate with four design variables and carbon fibre reinforcement which is 1.844 (Table 17).

Table 16
Fundamental frequencies of 8-layered skew ($a/b = 0.71$) and rectangular ($a/b = 1$) laminates with three design variables (GPLs and fibre contents, layer thickness ratios) and with $W_{GPLmax} = 0.0125$, $V_{Fmax} = 0.30$, $D/a = 0.03$.

Symmetric fibre orientation $[90°/0°/90°/0°]_s$								
Fibre type	Laminate type	W_{GPL}	V_F	h/D	Ω	Increase (%)	Ω_0	$\eta = \frac{\Omega}{\Omega_0}$
Glass	Rectangular (0°)	$[0.14/0.0/0.0/0.0]_s$	$[0.1/0.6/0.1/0.27]_s$	$[0.05/0.15/0.15/0.15]_s$	0.0036	–	0.0024	1.500
	45° Skew	$[0.13/0.0/0.0/0.0]_s$	$[0.10/0.60/0.27/0.10]_s$	$[0.05/0.15/0.15/0.15]_s$	0.0047	31%	0.0032	1.469
Carbon	Rectangular (0°)	$[0.14/0.0/0.0/0.0]_s$	$[0.1/0.6/0.1/0.27]_s$	$[0.05/0.15/0.15/0.15]_s$	0.0055	–	0.0032	1.719
	45° Skew	$[0.13/0.0/0.0/0.0]_s$	$[0.10/0.60/0.27/0.10]_s$	$[0.05/0.15/0.15/0.15]_s$	0.0065	18%	0.0042	1.548

Table 17
Fundamental frequencies of 8-layered skew ($a/b = 0.71$) and rectangular ($a/b = 1$) laminates with four design variables (GPLs and fibre contents, thickness ratios, fibre angles) and with $W_{GPLmax} = 0.0125$, $V_{Fmax} = 0.30$, $D/a = 0.03$.

Fibre type	Laminate type	W_{GPL}	V_F	h/D	θ	Ω	Increase (%)	Ω_0	$\eta = \frac{\Omega}{\Omega_0}$
Glass	Rectangular (0°)	$[0.037/0.0303/0.0/0.0]_s$	$[0.6/0.6/0.1/0.1]_s$	$[0.15/0.05/0.15/0.15]_s$	$[5/51/-20/88]_s$	0.0032	–	0.0024	1.333
	45° Skew	$[0.127/0.0/0.0/0.0]_s$	$[0.1/0.6/0.27/0.1]_s$	$[0.05/0.15/0.15/0.15]_s$	$[90/0/90/0]_s$	0.0047	47%	0.0032	1.469
Carbon	Rectangular (0°)	$[0.01/0.111/0.0/0.0]_s$	$[0.6/0.1/0.27/0.1]_s$	$[0.15/0.05/0.15/0.15]_s$	$[3/50/0/88]_s$	0.0059	–	0.0032	1.844
	45° Skew	$[0.027/0.045/0.0/0.0]_s$	$[0.6/0.1/0.27/0.1]_s$	$[0.15/0.05/0.15/0.15]_s$	$[-6/50/-18/88]_s$	0.0069	17%	0.0042	1.643

8. Conclusions

In the present study, maximizing the fundamental frequencies of graphene/fibre-reinforced cantilever skew laminates is studied. Design parameters include the distributions of the graphene and fibres across the laminate thickness, layer thicknesses and the fibre angles. To assess the effectiveness of different design variables in maximizing the fundamental frequency, the number of design variables is increased in steps. The effective material properties are calculated using micromechanics relations and the numerical solutions are obtained using finite element analysis based on the first-order shear deformation theory. For the implementation of the optimization scheme, a Sequential Quadratic Programming algorithm (SQP) is adopted.

Results indicate that the optimal, non-uniform distributions of the graphene and the fibres lead to higher contents in the outer layers and lower or zero reinforcement in the inner layers. This result is expected and is due to the outer layers contributing more to the stiffness of the laminates. In the case of the graphene being the only reinforcement in the optimization, diminishing returns were observed when the graphene content exceeds a certain limit and the design becomes less cost-effective.

When both graphene and fibre contents along the thickness are adopted as the two design variables and the upper limit on total fibre content is specified as 30%, a higher frequency is obtained as compared to the case with 60% uniform fibre content. Thus, the skew laminates can be designed cost effectively using lower fibre volume contents by distributing the fibres and the graphene across the thickness optimally.

Comparisons are given for the optimal designs of three-phase graphene/fibre-reinforced laminates (the present design) and the traditional two-phase laminates reinforced with fibres only. Results indicate a substantial increase in the fundamental frequency for the three-phase laminates as compared to the two-phase laminates. This increase is higher for glass fibre reinforcement (more than 45%) but is also very significant for carbon fibre reinforcement (more than 20%).

To provide a quantitative criterion for evaluating the results, a design efficiency factor is defined and calculated for each optimal design. Using this factor, optimal design results can be compared and the design efficiencies of different reinforcements can be assessed. The design efficiency increases when the number of design variables increases as expected and the highest design efficiency corresponds to the case with four design variables.

Finally, results for the optimal designs of rectangular and 45° skew plates are compared. It is shown that although the maximum fundamental frequency is higher for the 45° skew laminates, the design efficiency decreases compared to the rectangular laminates for most cases. The differences in the design efficiencies of these two laminate types depend on the number of design variables used in the optimization.

CRediT authorship contribution statement

Y. Jeawon: Writing – original draft, Visualization, Investigation, Formal analysis. **G.A. Drosopoulos:** Writing – review & editing, Supervision, Resources, Methodology, Data curation, Conceptualization. **G. Foutsitzi:** Validation, Software, Methodology, Data curation. **G.E. Stavroulakis:** Writing – review & editing, Resources, Data curation. **S. Adali:** Writing – review & editing, Methodology, Conceptualization.

Declaration of competing interest

The authors declare that they have no known competing financial interests or personal relationships that could have appeared to influence the work reported in this paper.

Data availability

Data will be made available on request

Acknowledgements

The research reported in this paper was supported by research grants from the University of KwaZulu-Natal (UKZN), South Africa and from National Research Foundation (NRF) of South Africa. The authors gratefully acknowledge the supports provided by UKZN, South Africa and NRF, UK.

References

[1] K.D. Rao, K.S. Babu, Modal analysis of thin FRP skew symmetric angle-ply laminate with circular cut-out, Int. J. Eng. Res. Technol. 1 (2012) 1–5.
[2] A. Mandal, C. Ray, S. Haldar, Free vibration analysis of laminated composite skew plates with cut-out, Arch. Appl. Mech. 87 (9) (2017) 1511–1523.
[3] W.H. Liu, W.C. Chen, Vibration analysis of skew cantilever plates with stiffeners, J. Sound Vib. 159 (1) (1992) 1–11.
[4] K. Hosokawa, J. Xie, T. Sakata, Free vibration analysis of cantilevered laminated trapezoidal plates, Sci. Eng. Compos. Mater. 8 (1999) 1–10.
[5] S. Chikkol Venkateshappa, Y.J. Suresh, W.P. Prema Kumar, Free flexural vibration studies on skew plates, Int. J. Aerosp. Lightweight Struct. 2 (2013) 405–420.
[6] A.K. Garg, R.K. Khare, T. Kant, Free vibration of skew fiber reinforced composite and sandwich laminates using a shear deformable finite element model, J. Sandw. Struct. Mater. 8 (1) (2006) 33–53.
[7] F. Gburi, L. Alansari, M. Kadhom, A. Al-Saffar, Free vibration of skew isotropic plate using ANSYS, J. Mech. Eng. Res. Dev. 43 (2020) 472–486.
[8] M. Gürses, Ö. Civalek, A.K. Korkmaz, H. Ersoy, Free vibration analysis of symmetric laminated skew plates by discrete singular convolution technique based on first-order shear deformation theory, Internat. J. Numer. Methods Engrg. 79 (3) (2009) 290–313.

[9] Y. Kiani, Free vibration of FG-CNT reinforced composite skew plates, Aerosp. Sci. Technol. 58 (2016) 178–188.
[10] C. Ömer, A. Mehmet, Free vibration and buckling analyses of CNT reinforced laminated non-rectangular plates by discrete singular convolution method, Eng. Comput. 38 (Suppl 1) (2022) S489–S521.
[11] E. García-Macías, R. Castro-Triguero, E. Saavedra Flores, M. Friswell, R. Gallego, Static and free vibration analysis of functionally graded carbon nanotube reinforced skew plates, Compos. Struct. 140 (2016) 473–490.
[12] L.W. Zhang, On the study of the effect of in-plane forces on the frequency parameters of CNT-reinforced composite skew plates, Compos. Struct. 160 (2017) 824–837.
[13] L. Zhang, Z. Lei, K. Liew, Vibration characteristic of moderately thick functionally graded carbon nanotube reinforced composite skew plates, Compos. Struct. 122 (2015) 172–183.
[14] E. García-Macías, R. Castro-Triguero, Coupled effect of CNT waviness and agglomeration: A case study of vibrational analysis of CNT/polymer skew plates, Compos. Struct. 193 (2018) 87–102.
[15] T. Farsadi, D. Asadi, H. Kurtaran, Fundamental frequency optimization of variable stiffness composite skew plates, Acta Mech. 232 (2020) 555–573.
[16] C.H. Thai, A.J.M. Ferreira, T.D. Tran, P. Phung-Van, Free vibration, buckling and bending analyses of multilayer functionally graded graphene nanoplatelets reinforced composite plates using the NURBS formulation, Compos. Struct. 220 (2019) 749–759.
[17] M. Song, S. Kitipornchai, J. Yang, Free and forced vibrations of functionally graded polymer composite plates reinforced with graphene nanoplatelets, Compos. Struct. 159 (2017) 579–588.
[18] F. Pashmforoush, Statistical analysis on free vibration behavior of functionally graded nanocomposite plates reinforced by graphene platelets, Compos. Struct. 213 (2019) 14–24.
[19] A. Shahrjerdi, S. Yavari, Free vibration analysis of functionally graded graphene-reinforced nanocomposite beams with temperature-dependent properties, J. Braz. Soc. Mech. Sci. Eng. 40 (2018) 25.
[20] Z. Xu, Q. Huang, Vibro-acoustic analysis of functionally graded graphene-reinforced nanocomposite laminated plates under thermal-mechanical loads, Eng. Struct. 186 (2019) 345–355.
[21] U. Topal, Ü. Uzman, Frequency optimization of laminated skew plates, Mater. Des. 30 (2009) 3180–3185.
[22] K. Kalita, P. Dey, S. Haldar, Robust genetically-optimized skew laminates, Proc. Inst. Mech. Eng. C J. Mech. Eng. Sci. 233 (1) (2018) 146–159.
[23] K. Kalita, Dey P., S. Haldar, X. Gao, Optimizing frequencies of skew composite laminates with metaheuristic algorithms, Eng. Comput. 36 (2020) 741–761.
[24] Y. Kiani, K. Kamil Zur, Free vibrations of graphene platelet reinforced composite skew plates resting on point supports, Thin-Walled Struct. 176 (2022) 109363.
[25] C. Feng, S. Kitipornchai, J. Yang, Nonlinear free vibration of functionally graded polymer composite beams reinforced with graphene nanoplatelets (GPLs), Eng. Struct. 140 (2017) 110–119.
[26] R.J. Young, M. Liu, I.A. Kinloch, S. Li, X. Zhao, C. Vallés, D.G. Papageorgiou, The mechanics of reinforcement of polymers by graphene nanoplatelets, Compos. Sci. Technol. 154 (2018) 110–116.
[27] Y. Jeawon, G.A. Drosopoulos, G. Foutsitzi, G.E. Stavroulakis, S. Adali, Optimization and analysis of frequencies of multi-scale graphene/fibre reinforced nanocomposite laminates with non-uniform distributions of reinforcements, Eng. Struct. 228 (2020) 111525.
[28] S.K. Georgantzinos, G.I. Giannopoulos, S.I. Markolefas, Vibration analysis of carbon fibre-graphene-reinforced hybrid polymer composites using finite element techniques, Materials 13 (2020) 4225.
[29] I.S. Radebe, G.A. Drosopoulos, S. Adali, Buckling of non-uniformly distributed graphene and fibre reinforced multiscale angle-ply laminates, Meccanica 54 (14) (2019) 1–17.
[30] JN. Reddy, Mechanics of Laminated Composite Plates and Shells, second ed., 2004, p. CRC Press.
[31] Y. Huang, Z. Yang, A. Liu, J. Fu, Nonlinear buckling analysis of functionally graded graphene reinforced composite shallow arches with elastic rotational constraints under uniform radial load, Materials 11 (6) (2018) 910.
[32] J. Yang, H. Wu, S. Kitipornchai, Buckling and post-buckling of functionally graded multilayer graphene platelet-reinforced composite beams, Compos. Struct. 161 (2017) 111–118.
[33] T. Vo-Duy, V. Ho-Huu, T.D. Do-Thi, H. Dang-Trung, T. Nguyen-Thoi, A global numerical approach for lightweight design optimization of laminated composite plates subjected to frequency constraints, Compos. Struct. 159 (2017) 646–655.
[34] H.-S. Shen, A comparison of buckling and post-buckling behavior of FGM plates with piezoelectric fibre reinforced composite actuators, Compos. Struct. 91 (2009) 375–384.
[35] M. Rafiee, F. Nitzsche, M.R. Labrosse, Modeling and mechanical analysis of multiscale fibre reinforced graphene composites: Nonlinear bending, thermal post-buckling and large amplitude, Int. J. Non-Linear Mech. 103 (2018) 104–112.
[36] R. Gholami, R. Ansari, Y. Gholami, Numerical study on the nonlinear resonant dynamics of carbon nanotube/fibre/polymer multiscale laminated composite rectangular plates with various boundary conditions, Aerosp. Sci. Technol. 78 (2018) 118–129.
[37] S. Kamarian, M. Shakeri, M.H. Yas, Natural frequency analysis and optimal design of CNT/fibre/polymer hybrid composites plates using Mori–Tanaka approach, GDQ technique, and firefly algorithm, Polym. Compos. 9 (5) (2016) 1433–1446.
[38] M. Song, J. Yang, S. Kitipornchai, W. Zhu, Buckling and postbuckling of biaxially compressed functionally graded multilayer graphene nanoplatelet-reinforced polymer composite plates, Int. J. Mech. Sci. 131–132 (2017) 345–355.
[39] Y. Wang, C. Feng, Z. Zhao, J. Yang, Eigenvalue buckling of functionally graded cylindrical shells reinforced with graphene platelets (GPL), Compos. Struct. 202 (2018) 38–46.
[40] Y. Wang, C. Feng, Z. Zhao, J. Yang, Buckling of graphene platelet reinforced composite cylindrical shell with cutout, Int. J. Struct. Stab. Dyn. 18 (03) (2018) 1850040.
[41] J. Nocedal, S.J. Wright, Numerical Optimization, in: Springer Series in Operations Research and Financial Engineering, 2006.
[42] Z.B. Zabinsky, Optimal design of composite structures, in: C.A. Floudas, P.M. Pardalos (Eds.), Encyclopaedia of Optimization, Kluwer Academic Publishers, 2001, pp. 153–160.
[43] P.Y. Papalambros, D.J. Wilde, Principles of Optimal Design, in: Modelling and Computation, Cambridge University Press, 2017.
[44] MATLAB, Version 9.0.0.341360 (R2016a), The MathWorks Inc, Natick, Massachusetts, 2016.
[45] AK. Garg, RK. Khare, T. Kant, Free vibration of skew fiber-reinforced composite and sandwich laminates using a shear deformable finite element model, J. Sandw. Struct. Mater. 8 (1) (2006) 33–53.
[46] O.G. McGee, Natural vibrations of shear deformable cantilevered skew thick plates, J. Sound Vib. 176 (3) (1994) 351–376.